Crystal Structure at 1.9 Å Resolution of the Apoovotransferrin N-Lobe Bound by Sulfate Anions: Implications for the Domain Opening and Iron Release Mechanism[†,‡]

Kimihiko Mizutani, Honami Yamashita, Bunzo Mikami, and Masaaki Hirose*

The Research Institute for Food Science, Kyoto University, Uji, Kyoto 611 0011, Japan

Received November 8, 1999; Revised Manuscript Received December 27, 1999

ABSTRACT: Several lines of functional evidence have shown that anion binding to a nonsynergistic site is a prerequisite for the anion-mediated iron release mechanism of transferrins. We report here structural evidence of the location of sulfate anion binding sites of the ovotransferrin N-lobe via the 1.90 Å resolution apo crystal structure. The crystals were grown in an ammonium sulfate solution and belonged to space group $P6_322$ with the following unit cell dimensions: $a = b = 125.17$ Å and $c = 87.26$ Å. The structural determination was performed by isomorphous replacement, using Pt and Au derivatives. The structure refinement gave an *R*-factor of 0.187 in the resolution range of 7.0−1.90 Å for the final model. From the electron density map, the existence of four bound SO_4^{2-} anions was detected. Three of them that exhibited reasonably low *B*-factors were all located in the opened interdomain cleft (sites 1−3). In site 1, the bound anion directly interacts with an Fe^{3+}-coordinating ligand; SO_4 O1 and SO_4 O3 form hydrogen bonds with His250 NE2. Oxygen atom O3 of the same sulfate anion makes a hydrogen bond with Ser91 OG in a hinge strand. The sulfate anion in site 2 partially occupies the synergistic anion binding sites; SO_4 O2 and SO_4 O3 are hydrogen bonded to Arg121 NE and NH2, respectively, both of which are consensus anchor groups for CO_3^{2-} anion in holotransferrins. The former oxygen atom of SO_4^{2-} is also hydrogen bonded to Ser122 N, which forms a hydrogen bond with Fe^{3+}-coordinating ligand Asp60 OD2 in holotransferrins. Some of the SO_4^{2-} oxygen atoms in sites 1 and 2 interact indirectly through H_2O molecules with functionally important protein groups, such as the other Fe^{3+}-coordinating ligands, Tyr92 OH and Tyr191 OH, and a dilysine trigger group, Lys209 NZ. In site 3, SO_4 O1 and SO_4 O4 form hydrogen bonds with Ser192 OG and Tyr191 N, respectively, and SO_4 O2 forms hydrogen bonds with Ser192 N and Ser192 OG. These structural data are consistent with the view that the anion bindings to the interdomain cleft, especially to sites 1 and 2, play crucial roles in the domain opening and synergistic carbonate anion release in the iron release mechanism of the ovotransferrin N-lobe.

Transferrins are a homologous group of iron-binding proteins that include serum transferrin, ovotransferrin, and lactoferrin (*1*). These proteins serve to control the levels of iron in the body fluids of vertebrates via their ability to bind two Fe^{3+} ions together very tightly with two CO_3^{2-} anions (*1*). Serum transferrin and ovotransferrin can act as an iron transporter to target cells. The transferrin-dependent Fe^{3+} delivery to the target cells occurs in such a way that the diferric transferrin first binds with the specific receptor that resides on the plasma membrane (*2*). The transferrin−receptor complex is then internalized into the cell, and the complex releases Fe^{3+} at acidic pH in the endosome (*2*). In vitro, the release of Fe^{3+} from ferric transferrins requires the presence of a simple anion, such as pyrophosphate, sulfate, and chloride, although the effect of anion on Fe^{3+} release kinetics is significantly different between the two ferric binding sites (*3*−*8*). The requirement of an anion for Fe^{3+} release has been also demonstrated for the Fe^{3+}−transferrin−receptor complex (*9*). The cellular Fe^{3+} release may, therefore, be regulated by some anion.

The ∼80 kDa transferrin molecule consists of two similarly sized homologous N- and C-lobes, which are further divided into two similarly sized domains (N1 and N2 in the N-lobe and C1 and C2 in the C-lobe). The two iron-binding sites are located within the interdomain cleft of each lobe. Crystal structures of the fully iron-loaded diferric forms (*10*−*15*) and the monoferric N-lobes (*16*−*19*) of several transferrins reveal that the two domains of each lobe are closed over an Fe^{3+} ion. Four of the six Fe^{3+} coordination sites are occupied by protein ligands (two Tyr residues, one Asp residue, and one His residues) and the other two by a bidentate carbonate anion. Previous kinetic studies have, however, strongly suggested that anion binding to transferrins promotes a structural change of the closed holo form that is an absolute prerequisite for Fe^{3+} release (*5*, *7*, *20*, *21*). In the Fe^{3+}-free apo form, all the lobes of iron transporter transferrins assume a conformation with an opening of the interdomain cleft, as revealed by X-ray crystallographic (*22*−

[†] This work was supported in part by a grant-in-aid for scientific research from the Ministry of Education, Science, Sports and Culture of Japan.

[‡] The atomic coordinates of the apo structure (1TFA) have been deposited with the Protein Data Bank, Research Collaboratory for Structural Bioinformatics, Rutgers University, New Brunswick, NJ.

* To whom correspondence should be addressed. Telephone: 81-774-38-3734. Fax: 81-774-38-3735. E-mail: hirose@soya.food.kyoto-u.ac.jp.

10.1021/bi992574q CCC: $19.00
Published on Web 03/03/2000

24) and solution scattering (*25*−*28*) analyses. These structural and functional results imply that the anion-induced Fe^{3+} release by transferrins is closely related to the opening of the domains. The location of the anion binding site which should be crucial knowledge for the understanding of the anion-induced domain opening and iron release mechanism remains, however, to be established.

In the study presented here, the ovotransferrin N-lobe has been crystallized in an ammonium sulfate solution and the crystal structure has been determined at 1.9 Å resolution by the isomorphous replacement method. We report here the direct evidence for the presence of three nonsynergistic SO_4^{2-} binding sites (sites 1−3) in the interdomain cleft that is wide open as compared to the holo cleft structure (*17*). The sulfate anion in site 1 forms hydrogen bonds with an Fe^{3+}-coordinating ligand His250 NE and with Ser91 OG in a hinge strand. The sulfate anion in site 2 partially occupies the synergistic anion binding sites (Arg121 NE and NH2) and is also hydrogen bonded to Ser122 N. In site 3, SO_4^{2-} forms hydrogen bonds with Ser192 OG and N and with Tyr191 N. The functionally important situations of the residues in sites 1 and 2 strongly suggest that anion bindings to these sites play crucial roles for the domain opening and synergistic carbonate anion release in the iron release mechanism of the ovotransferrin N-lobe. A large movement in the side chain orientation of Ser91, when compared between the holo and SO_4^{2-}-bound apo structures, further supports the implications of site 1 for the anion-induced domain opening mechanism.

EXPERIMENTAL PROCEDURES

Crystallization. The hen ovotransferrin N-lobe (the N-terminal half-molecule) was isolated and purified as reported previously (*29*). The apo form of the protein was crystallized using the hanging-drop vapor-diffusion method. The solution in the crystallization drop was prepared, on a silanized coverslip, by mixing 5 μL of a 44.4 mg/mL protein solution [0.05 M Bis-Tris buffer (pH 6.0)] with 5 μL of a precipitant solution [52−53% ammonium sulfate (pH 6.0) and 0.05 M Bis-Tris buffer]. The droplets were equilibrated against 1 mL of the precipitant solution at 20 °C. Crystals were obtained within 1 month.

The apo crystals were subjected to diffraction experiments, using a Nonius precession camera with Ni-filtered CuKα radiation generated by a Rigaku X-ray generator (40 kV and 20 mA). The precession photographs indicated that the apo crystal belongs to space group $P6_322$ with the following cell dimensions: $a = b = 125.17$ Å and $c = 87.26$ Å.

Data Collection and Processing. Diffraction data were collected using CuKα radiation ($\lambda = 1.5418$ Å) with a Bruker Hi-star area detector coupled to a Mac Science M18XHF rotating-anode generator. A total of 194 748 reflections were collected to 1.83 Å resolution. The data were processed, scaled, and merged with Saint (Bruker Analytical X-ray Instruments, Inc., Madison, WI). For multiple isomorphous replacement (MIR), crystals were soaked for 1 h at 20 °C in the precipitant solution containing 0.2 mM PCMBS, 2 mM K_2PtCl_4, 5 mM $Sm_2(SO_4)_3$, 2 mM HgMeOH, 5 mM $KAu(CN)_2$, 5 mM $Pr(NO_3)_3$, or 10 mM $SmCl_3$. A number of heavy atom derivative data sets were collected and processed in the same way. Only K_2PtCl_4 and $KAu(CN)_2$ derivatives were, however, useable for MIR phasing. Details of the crystal parameter and statistics of the data sets are given in Table 1. One Pt binding site and two Au binding sites were obtained with the difference Patterson method using PHASES. The obtained MIR phase was improved by solvent flattening with PHASES. Statistics of the phasing appear in Table 1. An electron density map was made with the solvent-flattened MIR phase using the data between 15.0 and 3.0 Å. Domains 1 and 2 of the holo form of the ovotransferrin N-lobe (1NNT, 2.3 Å resolution) were translated and rotated to fit the map, respectively, using TURBO-FRODO.

Table 1: Summary of Data Collection and Refinement[a]

	native	K_2PtCl_4	$KAu(CN)_2$
(a) crystal data			
space group	$P6_322$	$P6_322$	$P6_322$
cell dimensions			
a (Å)	125.17	124.89	124.75
b (Å)	125.17	124.89	124.75
c (Å)	87.26	87.27	87.29
V_m (Å^3/Da)	2.7		
no. of molecules per asymmetric unit	1		
no. of observed reflections	194748	69684	62370
resolution (Å)	1.83	2.35	2.47
no. of independent reflections	34673	16471	14213
completeness (%)	95.5	94.9	94.8
R_{sym} (%)	6.3	7.3	9.7
phasing (∞−3.0 Å)			
R_{culis}		0.694	0.601
R_{kraut}		0.068	0.080
no. of heavy atoms		1	2
phasing power		1.25	1.47
figure of merit	0.491		
figure of merit after solvent flattening	0.816		
(b) refinement statistics			
resolution limits (Å)	7.0−1.9		
no. of reflections used [$F > 2\sigma(F)$]	27751		
completeness (%)	88.1		
no. of protein atoms	2543		
no. of solvent molecules	255		
ions	$4SO_4^{2-}$		
final *R*-factor	0.187		
R_{free}	0.243		
average *B*-factor (Å^2)	22.8		
rms deviation from standard geometry			
bond distances (Å)	0.012		
bond angles (deg)	2.88		
dihedrals (deg)	24.2		
improper dihedrals (deg)	1.12		

[a] Native is the apo crystal without the soaking with a metal ion. K_2PtCl_4 and $KAu(CN)_2$ represent the crystals soaked with K_2PtCl_4 and $KAu(CN)_2$, respectively. Phasing parameters were calculated at ∞−3.0 Å resolution.

Structure Refinement. The initial model made using the MIR map and the structure of the holo form was refined by simulated annealing with molecular dynamics using a slow-cooling protocol from 3000 to 300 K. This refinement yielded an *R* of 0.265 for the data between 15.0 and 2.5 Å resolution. Subsequent restrained least-squares refinement yielded an *R* of 0.243 for the same resolution. Several rounds of restrained least-squares refinement up to the resolution of 1.9 Å, followed by manual model building, were carried out to improve the model. Four sulfate anions and water molecules having more than 4σ on the $F_o - F_c$ map were then added to the model. The alternate side chain positions for the disorders at Asp25, Gln28, Lys100, Arg172, and Lys296 were added to the model in the final step of the refinement. The final model consisted of 329 amino acid residues, four sulfate anions, and 255 water molecules with

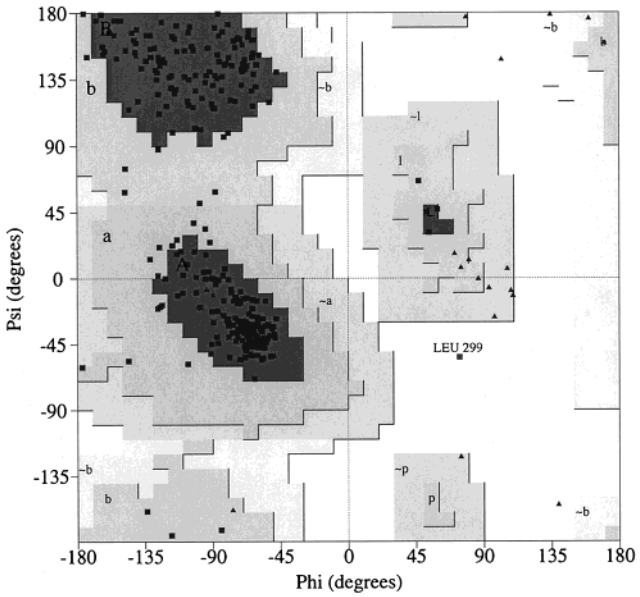

FIGURE 1: Ramachandran plot of the backbone torsion angles. Glycine residues are represented by triangles and non-glycine residues by squares. The γ-turn residue, Leu299, is labeled.

an R value of 0.187 (R_{free} = 0.243) for 27 751 reflections with F being greater than $2\sigma(F)$ between 7 and 1.9 Å resolution (Table 1).

The electron density maps ($2F_o - F_c$, contoured at 1σ) were calculated using the reflection data at 7.0−1.9 Å resolution. The omit maps ($F_o - F_c$, contoured at 3σ) were obtained from the model in which sulfate molecules were excluded.

RESULTS

Quality of the Refined Model. Residues 1−3 are not included in the model, because no clearly interpretable electron density could be seen. To the side chains of residues at positions 25, 28, 100, 172, and 296 were added alternate models to fit the disordered side chains. Relevant refinement statistics are given in Table 1. The overall completeness, R-factor, and R_{free} were 88.1%, 0.187, and 0.243, respectively, for the data where $F > 2\sigma(F)$. For the highest-resolution bin (1.90−1.98 Å), the completeness was 70.2%, and the R-factor and R_{free} were 0.275 and 0.294, respectively. From a Luzzati plot, the mean absolute error in atomic position is estimated to be 0.22 Å.

Table 2: *B*-Factors for the Bound Anion Atoms

	B-factor for the sulfate atoms (Å^2)				
anion	S	O1	O2	O3	O4
sulfate 351	37.35	41.25	37.30	38.81	36.76
sulfate 352	48.64	52.41	50.65	48.60	48.47
sulfate 353	51.12	53.77	53.80	52.48	51.28
sulfate 354	75.25	72.88	74.74	71.81	75.17

A Ramachandran plot (*30*) of the main chain torsion angles is shown in Figure 1. The main chain conformational angles show that about 89.3% lie within the core region, with 99.7% lying within the allowed region. One non-glycine residue (Leu299) lies outside the allowed regions of conformational space; it is in a γ-turn. The other non-glycine residue (Trp125) lies on the edge of the additional allowed region of α-helix; it is in a distorted α-helix caused by Gly124 and Pro128.

Overall Organization of the Structure. Figure 2 displays the overall structure of the apoovotransferrin N-lobe as a Cα trace. The apo structure, when compared with the previous holo (the Fe^{3+}- and CO_3^{2-}-loaded form) structure of the ovotransferrin N-lobe (*17*), comprises a domain-opened conformation (Figure 2). The mode and extent of the opening were almost the same as in the N-lobe of the full-length molecule of ovotransferrin (*24*); as calculated by the rigid-body motion method (*31*), the domains move 49.7° around a rotation axis passing through the two β-strands linking the domains.

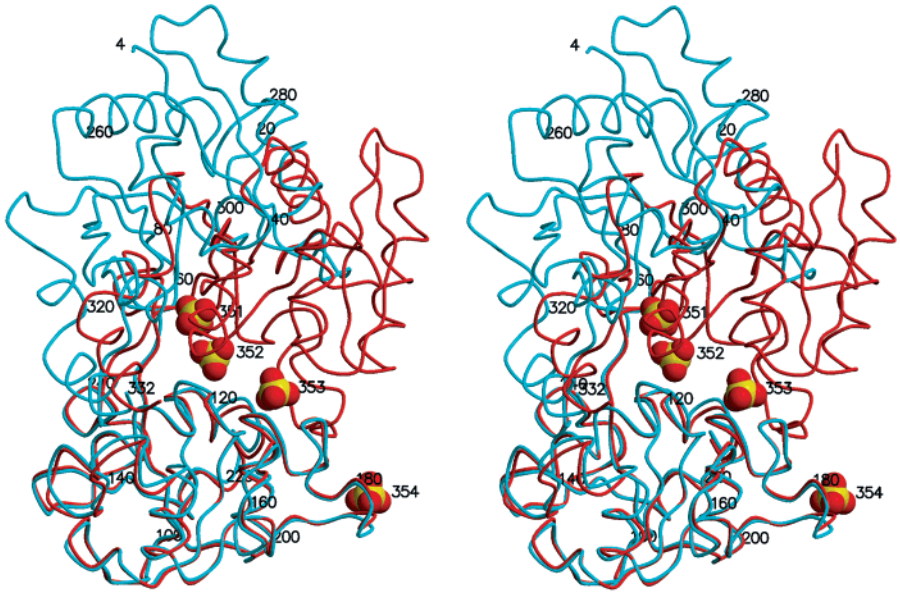

FIGURE 2: Stereo Cα plots of the apo (cyan) and holo forms (red) of the ovotransferrin N-lobe. The figures were produced with MOLSCRIPT (*43*) and Raster3D (*44*) as the superimposed ones on domain N2. The holo structure is drawn using the previously determined data (PDB file 1NNT) (*17*). The residue numbers are labeled for the apo form. The sulfur and oxygen atoms of bound sulfate anions are shown as yellow and red spheres, respectively. Sulfate anions 351−353 correspond to the anions in sites 1−3, respectively.

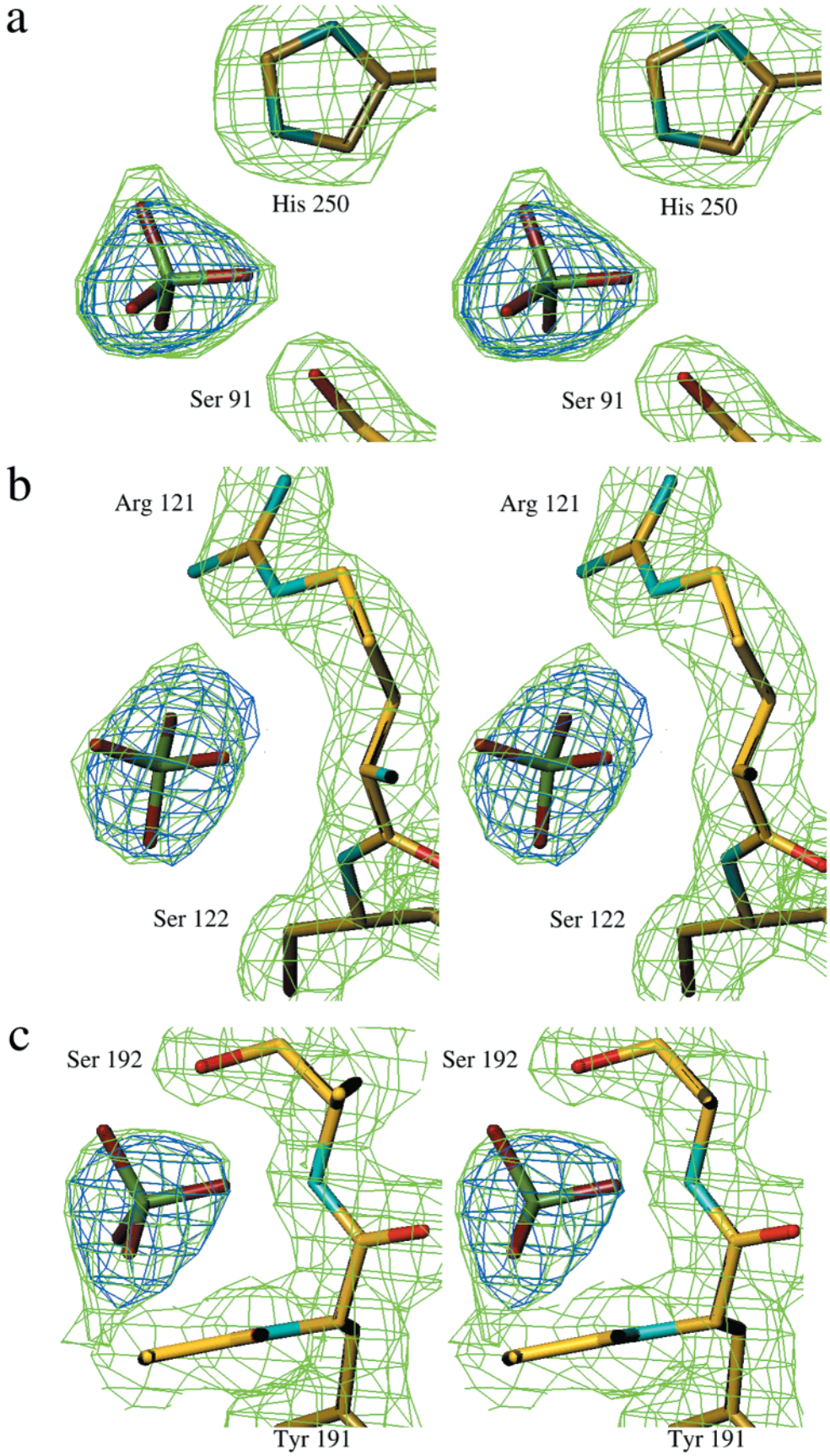

FIGURE 3: Stereoviews depicting the sulfate binding sites. Electron density maps (green, $2F_o - F_c$, contoured at 1σ) were calculated for site 1 (a), site 2 (b), and site 3 (c). The omit maps (blue, $F_o - F_c$, contoured at 3σ) were obtained from the model in which sulfate molecules were omitted. The final model is superimposed in a stick representation with atoms in standard colors.

One of the most important observations depicted in Figure 2 is that the bindings of four sulfate anions are clearly detected from an electron density map. Three of the bound anions are located in the interdomain cleft (sulfates 351−

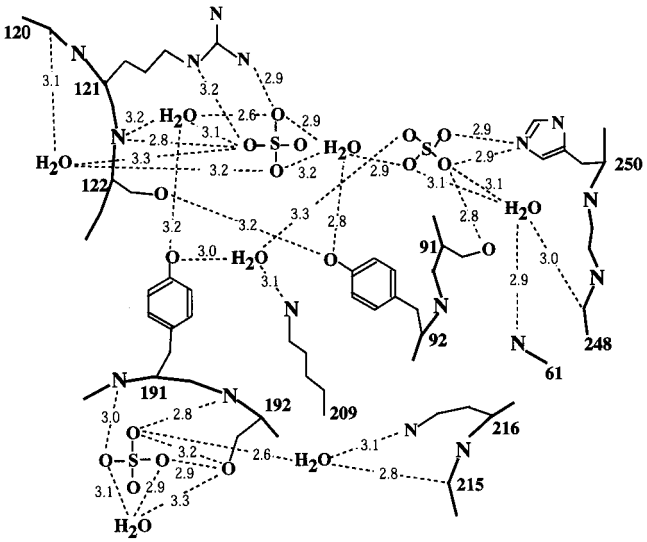

FIGURE 4: Diagram of the hydrogen bonding network around the three sulfate anion binding sites in the interdomain cleft. The dotted lines display hydrogen bonds with the bond distances in angstroms.

353), while the other one (sulfate 354) exists outside the cleft. None of the four anions participated in the intermolecular interactions in the crystal packing. Table 2 summarizes *B*-factors for the oxygen and sulfur atoms of the four bound anions. The lowest *B*-factors were found for sulfate 351; the values ranged from 37 to 41 Å^2 for the five atoms of SO_4^{2-}. The atoms of sulfate 352 exhibited the second smallest values, which ranged from 48 to 52 Å^2. Sulfate 353 had slightly larger values, which ranged from 51 to 54 Å^2, than sulfate 352. Sulfate 354 exhibited much larger values than the other three sulfate anions; the values ranged from 72 to 75 Å^2, suggesting highly mobile and/or a less tight binding nature of SO_4^{2-} located outside the interdomain cleft.

Structures of Anion Binding Sites. Figure 3 displays stereodiagrams of the electron density maps (green, $2F_o - F_c$) for the three sulfate anions located in the interdomain cleft. The figure also shows the omit maps (blue, $F_o - F_c$) calculated with the exclusion-of-sulfate model and demonstrates that three sulfate anions are detected with clear electron densities in the interdomain cleft. As shown in panel a, sulfate 351 exists in proximity to the side chains of His250 and Ser91; we name this anion binding site site 1. Sulfate 352 exists in proximity to the main chain of Ser122 and to the side chain of Arg121, constituting site 2 (panel b). As site 3, sulfate 353 exists in proximity to a main chain group of Tyr191 and main chain and side chain groups of Ser192 (panel c).

Figure 4 illustrates the hydrogen bonding structures for the three anion binding sites. In site 1, SO_4 O1 and SO_4 O3 form hydrogen bonds with His250 NE2, which is an iron-coordinating protein group (*11*, *17*). Oxygen atom O3 of the same sulfate anion makes a hydrogen bond with Ser91 OG.

In site 2, SO_4 O2 and SO_4 O3 are hydrogen bonded to Arg121 NE and NH2, respectively, both of which form hydrogen bonds with synergistic carbonate anion in the holo structure (*11*, *17*). The former oxygen atom of SO_4^{2-} is also hydrogen bonded to Ser122 N, which forms a hydrogen bond with Asp60 OD2 in the holo structure (*11*, *17*).

In site 3, SO_4 O4 and SO_4 O1 form hydrogen bonds with Tyr191 N and Ser192 OG, respectively, and SO_4 O2 receives two hydrogen bonds from Ser192 N and Ser192 OG.

Table 3: Surface Accessibilities of the Atoms in the Anion Binding Sites

	accesibility (Å^2)	
atom	holo form[a]	apo form[b]
site 1		
Ser91 OG	5.99	10.43
His250 NE	0.00	12.09
site 2		
Ser122 N	0.00	5.90
Arg121 NE	0.88	9.68
Arg121 NH2	18.38	50.97
site 3		
Tyr191 N	0.00	3.76
Ser192 N	0.67	2.44
Ser192OG	1.09	28.99

[a] The values were obtained using the previously determined data (PDB file 1NNT) (*17*). [b] For calculation of the accessibility, SO_4^{2-} anions are excluded from the model.

The three sulfate anions also make hydrogen bonds with seven H_2O molecules (Figure 4). Interestingly, three of the H_2O molecules, which form hydrogen bonds with the sulfate anions in sites 1 and 2, simultaneously make different hydrogen bonds with functionally important protein groups; a H_2O molecule forming hydrogen bonds with O2 and O3 of the sulfate at site 2 also makes hydrogen bonds with Ser122 N and with an iron-coordinating group, Tyr191 OH. Another H_2O molecule being hydrogen-bonded to O2 of the site 1 sulfate receives hydrogen bonds from an iron-coordinating group, Tyr191 OH, and from a dilysine trigger group, Lys209 NZ. The last H_2O molecule, which forms hydrogen bonds with O3 and O4 of the site 2 sulfate and with O4 of the site 1 sulfate, simultaneously forms a hydrogen bond with another iron-coordinating group, Tyr92 OH.

Surface Accessibilities of the Protein Groups in the Anion Binding Sites. The surface accessibilities of the atoms of the anion binding protein groups of sites 1−3 were calculated and compared with those in the holo structure (*17*). As summarized in Table 3, all the anion binding atoms exhibited greatly increased accessibility in the apo structure compared to the holo structure. The three sites are all localized in the Fe^{3+}-binding interdomain cleft. These strongly suggest that the anion binding to these sites is closely related to the domain opening in the ovotransferrin N-lobe.

DISCUSSION

In the study described here, the apo structure of the ovotransferrin N-lobe has been determined at 1.9 Å resolution with an *R*-factor of 0.187. This model is the highest-resolution structure for the apotransferrins determined to date (*22*−*24*, *32*−*34*) and provides important insight into the iron release mechanism of the N-lobe of transferrins.

The rate for iron release from transferrin is known to be accelerated by several factors, including endosomal low pH (*35*), association with the specific receptor at acidic pH (*36*), and binding of simple nonsynergistic anions (*3*−*8*). As an iron release mechanism at low pH from the N-lobes of iron transporter transferrins, the protonation mechanism of the "dilysine trigger" has been proposed on the basis of the ovotransferrin N-lobe holo structure (*17*); the two lysine residues Lys209 NZ and Lys301 NZ, which are located on the opposite domains of the protein, are separated by only

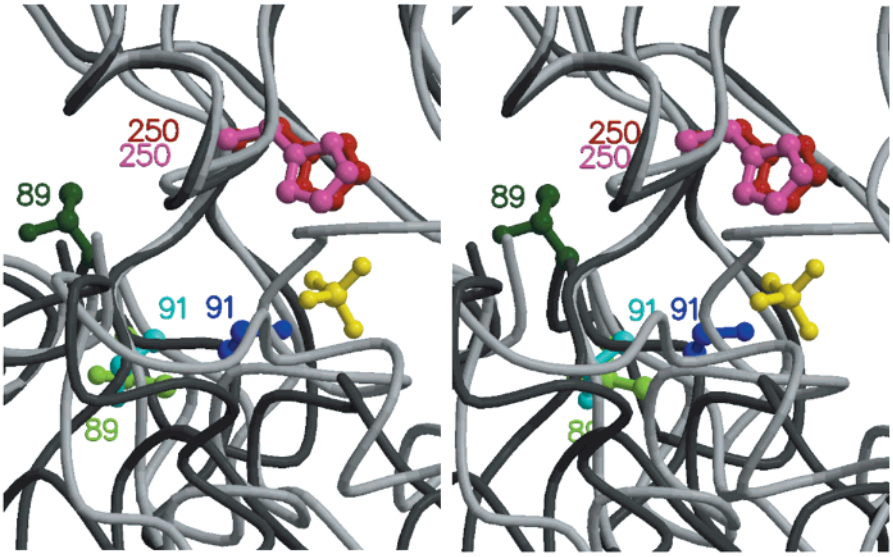

FIGURE 5: Stereodiagrams of site 1 residues. The figures are produced with MOLSCRIPT (*43*) and Raster3D (*44*) as superimposed on N1 domains of the apo and holo structures. The holo structure is drawn using the previous data (PDB file 1NNT) (*17*). Upper and lower halves are domain N1 and domain N2, respectively, and the right side between the two domains corresponds to the cleft. The apo and holo structures are shown in dark and light colors, respectively: Cα trace in gray, His250 in red, Ser91 in blue, and Thr89 in green. The sulfate molecule is shown in yellow.

2.3 Å. This mechanism has been supported by the functional evidence which shows that the rate of iron release from the human serum transferrin N-lobe is much slower in dilysine (Lys206−Lys296) mutants than in the wild-type protein counterpart (*37*−*39*). According to the apo structure described here, the Lys209 NZ−Lys301 NZ distance is 7.6 Å. The interaction of the two lysine residues is therefore abolished in the iron-released, domain-opened apo structure, which further supports the dilysine trigger mechanism. As an alternative factor, the requirement of a simple anion or anion chelator for the iron release has been demonstrated either for the N-teminal monoferric serum transferrin (*3*, *5*, *6*) and ovotransferrin (*4*) or for the isolated N-lobe of serum transferrin (*38*, *39*). Likewise, the iron release from the isolated N-lobe of ovotransferrin is facilitated by the presence of a simple anion, including sulfate anion (B. K. Muralidhara and M. Hirose, unpublished results). Then, a question about whether anion-dependent iron release is directly related to the dilysine trigger mechanism has been raised. Results from the site-directed mutagenesis studies by Woodworth and his collaborators (*39*, *40*) have suggested the participation of the dilysine residues as anion binding sites, on the basis of anion titration analyses and Fe^{3+} release kinetics of Lys206 and Lys296 mutants. The results from the ion release kinetics by other laboratories are, however, inconsistent with the view that these two lysine residues are part of anion binding sites for anion-dependent iron release (*37*, *38*). Such controversial situations have probably been due to the absence of direct structural evidence for nonsynergistic anion binding sites in transferrins.

For the crystallographic analysis of anion binding sites of transferrins, the use of the apo forms is considered appropriate, since the addition of anion to the holo forms should trigger the iron release reaction that accompanies a conformational change. In previous reports, the apotransferrin structure has been determined with the full-length molecules of lactoferrin (*32*−*34*) and ovotransferrin (*22*, *24*), and with the N-lobe of human serum transferrin (*23*). In these studies, crystals have been grown in nonanionic precipitants, including ethanol (*34*), 2-methyl-2,4-pentanediol and ethanol (*23*, *32*, *33*), and polyethylene glycol (*24*). Under these precipitant conditions, no attempt has been made to crystallize apotransferrin saturated with nonsynergistic anion. This study is the first example that utilizes ammonium sulfate as a precipitant for apo crystal growth. The results from this study clearly demonstrate the presence of four bound SO_4^{2-} anions in the apo crystal structure. The absence of bound anion in either Lys209 NZ or Lys301 NZ rules out the direct implication of the dilysine residues for the anion-dependent iron release mechanism. However, a H_2O molecule that makes a hydrogen bond with Lys209 NZ is also hydrogen bonded to coordinating ligand Tyr191 OH as well as to SO_4 O2 of site 1 (Figure 4). Two other H_2O molecules that form hydrogen bonds with the sulfate anions of sites 1 and 2 also make hydrogen bonds with Tyr92 OH and Tyr191 OH (Figure 4). Recent structural evidence for an iron-loaded open form of the ovotransferrin N-lobe (*41*) demonstrates that Tyr92 OH and Tyr191 OH are the only iron-coordinating protein ligands in an intermediate state of ion binding and release. If the entry of the water molecules into the Tyr groups facilitates iron release, then Lys209 NZ may be indirectly involved in the iron release mechanism. Previous observation (*42*) of decreased iron release rates in a tyrosine-ligand mutant of human serum transferrin (Tyr95His mutation) can be accounted for by this context, if the replacement of the coordinating Tyr with His abolishes the hydrogen bonding network through H_2O molecules.

The current findings that three (sites 1−3) of the four SO_4^{2-} binding sites are all located in the interdomain cleft support more direct participation of anion binding in the iron release mechanism. The surface accessibilities of the protein groups of these sites are greatly increased by domain opening (Table 3). It is therefore very likely that the anion bindings to the three sites stabilize the open conformation. Furthermore, structural details strongly suggest that sites 1 and 2 play especially important roles in domain opening and/or release of the synergistic carbonate anion, since these two

sites include the protein groups that make functionally important interactions.

Site 1 includes Ser91 OG and His250 NE2. The latter protein group is a consensus Fe^{3+}-coordinating ligand (*10*−*19*). Furthermore, both Ser91 and His250 are localized in the hinge strands (strands e and j, respectively) (*11*) which can undergo a conformational change upon domain opening and closure. As shown in Figure 5, Ser91 OG faces almost opposite the interdomain cleft and may form a hydrogen bond with Thr89 OG1 with an oxygen−oxygen distance of 3.4 Å in the holo structure (*17*), but in the apo structure presented here, the group faces to the cleft and the hydrogen bond is disrupted with an increased Ser91 OG−Thr89 OG1 distance of 10.4 Å. In contrast, the Ser91 OG−His250 NE2 distance, which is 11.9 Å in the holo N-lobe, is shortened to 5.3 Å in the apo form so that these two protein groups interact through a sulfate anion bridge (Figures 4 and 5). Ser91 OG of site 1 has a partially surface accessible nature in the holo structure (Table 3). The Ser91 OG−Thr89 OG1 interaction in the holo structure may be disrupted by the anion binding to the former group, which works as a trigger for the domain opening that includes the above-mentioned structural transition of hinge.

The occupation of site 2 by anion may facilitate both the domain opening and carbonate anion release. Site 2 comprises Ser122 N, Arg121 NE, and Arg121 NH2 (Figures 3 and 4). Arg121 NE and Arg121 NH2 are consensus CO_3^{2-} anchor groups for holotransferrins (*10*−*19*). Anion binding to site 2 may therefore facilitate the release of the carbonate anion from transferrin. A protein group, Ser122 N, forms a hydrogen bond in the holo structure (*17*) with an oxygen atom (OD1) of Asp60; the Asp residue is the only iron-coordinating ligand from domain 1 and plays a central role in domain opening and closure (*26*). The anion binding to site 2 should, therefore, disrupt the Ser122 N−Asp60 interaction, facilitating domain opening. Taken together, it can be reasonably hypothesized that the cooperative anion binding to sites 1 and 2 induces a domain opening and carbonate anion release, and hence iron release.

In conclusion, hypothetical mechanisms for anion-dependent Fe^{3+} release that was originally proposed by Bates and co-workers (*20*, *21*) include domain opening and the replacement of CO_3^{2-} by an incoming anion. Although the intensive studies by site-specific mutation analyses have been carried out, the specific residues involved in anion binding have remained largely obscure. The crystal structure described here provides direct evidence for the anion binding sites in the ovotransferrin N-lobe. Furthermore, the structural details for sites 1 and 2 are closely related to the anion-dependent iron release mechanism in which a domain opening and CO_3^{2-} release are the prerequisites. Although the current anion binding structure is restricted to the case of sulfate anion, sites 1 and 2 comprise the positive charge residues, His250 and Arg121. It is very likely that the basic nature of these sites accommodates the bindings of a wide variety of simple anions.

ACKNOWLEDGMENT

We thank Dr. B. K. Muralidhara (Kyoto University) for his critical reading of this paper. Computational time was provided by the Super-Computer Laboratory, Institute for Chemical Research, Kyoto University.

REFERENCES

1. Aisen, P., and Listowsky, I. (1980) *Annu. Rev. Biochem. 49*, 357−393.
2. Klausner, R. D., Ashwell, G., van Renswoude, J., Harford, J. B., and Bridges, K. R. (1983) *Proc. Natl. Acad. Sci. U.S.A. 80*, 2263−2266.
3. Baldwin, D. A., and de Sousa, D. M. R. (1981) *Biochem. Biophys. Res. Commun. 99*, 1101−1107.
4. Cheuk, M. S., Keung, W. M., and Loh, T. T. (1987) *J. Inorg. Biochem. 30*, 121−131.
5. Kretchmar, S. A., and Raymond, K. N. (1988) *Inorg. Chem. 27*, 1436−1441.
6. Egan, T. J., Ross, D., Purves, L. R., and Adams, P. A. (1992) *Inorg. Chem. 31*, 1994−1998.
7. Nguyen, S. A. K., Craig, A., and Raymond, K. N. (1993) *J. Am. Chem. Soc. 115*, 6758−6764.
8. Bailey, C. T., Byrne, C., Chrispell, K., Molkenbur, C., Sakett, M., Reid, K., McCollum, K., Vibbard, D., and Catelli, R. (1997) *Biochemistry 36*, 10105−10108.
9. Egan, T. J., Zak, O., and Aisen, P. (1993) *Biochemistry 32*, 8162−8167.
10. Bailey, S., Evans, R. W., Garratt, R. C., Gorinsky, B., Hasnain, S., Horsburgh, C., Jhoti, H., Lindley, P. F., Mydin, A., Sarra, R., and Watson, J. L. (1988) *Biochemistry 27*, 5804−5812.
11. Kurokawa, H., Mikami, B., and Hirose, M. (1995) *J. Mol. Biol. 254*, 196−207.
12. Haridas, M., Anderson, B. F., and Baker, E. N. (1995) *Acta Crystallogr. D51*, 629−646.
13. Rawas, A., Muirhead, H., and Williams, J. (1996) *Acta Crystallogr. D52*, 631−640.
14. Moore, S. A., Anderson, B. F., Groom, G. R., Haridas, M., and Baker, E. N. (1997) *J. Mol. Biol. 274*, 222−236.
15. Sharma, A. K., Paramasivam, M., Srinivasan, A., Yadav, M. P., and Singh, T. P. (1999) *J. Mol. Biol. 289*, 303−317.
16. Sarra, R., Garratt, R., Gorinsky, B., Jhoti, H., and Lindley, P. (1990) *Acta Crystallogr. B46*, 763−771.
17. Dewan, J. C., Mikami, B., Hirose, M., and Sacchettini, J. C. (1993) *Biochemistry 32*, 11963−11968.
18. Day, C. L., Anderson, B. F., Tweedie, J. W., and Baker, E. N. (1993) *J. Mol. Biol. 232*, 1084−1100.
19. MacGillivray, R. T. A., Moore, S. A., Chen, J., Anderson, B. F., Baker, H., Luo, Y., Bewley, M., Smith, C. A., Murphy, M. E. P., Wang, Y., Mason, A. B., Woodworth, R. C., Brayer, G. D., and Baker, E. N. (1998) *Biochemistry 37*, 7919−7928.
20. Cowart, R. E., Kojima, N., and Bates, G. W. (1982) *J. Biol. Chem. 257*, 7560−7565.
21. Cowart, R. E., Swope, S., Loh, T. T., Chasteen, N. D., and Bates, G. W. (1986) *J. Biol. Chem. 281*, 4607−4614.
22. Rawas, A., Muirhead, H., and Williams, J. (1997) *Acta Crystallogr. D53*, 464−468.
23. Jeffrey, P. D., Bewley, M. C., MacGillivray, T. A., Mason, A. B., Woodworth, R. C., and Baker, E. N. (1998) *Biochemistry 37*, 13978−13986.
24. Kurokawa, H., Dewan, J. C., Mikami, B., Sacchettini, J. C., and Hirose, M. (1999) *J. Biol. Chem. 274*, 28445−28452.
25. Grossmann, J. G., Neu, M., Pantos, E., Schwab, F. J., Evans, R. W., Townes-Andrews, E., Lindley, P. F., Appel, H., Thies, W.-G., and Hasnain, S. S. (1992) *J. Mol. Biol. 225*, 811−819.
26. Grossmann, J. G., Neu, M., Evans, R. W., Lindley, P. F., Appel, H., and Hasnain, S. S. (1993) *J. Mol. Biol. 229*, 585−590.
27. Mecklenburg, S. L., Donohoe, R. J., and Olah, G. A. (1997) *J. Mol. Biol. 270*, 739−750.
28. Grossmann, J. G., Crawley, J. B., Strange, R. W., Patel, K. J., Murphy, L. M., Neu, M., Evans, R. W., and Hasnain, S. S. (1998) *J. Mol. Biol. 279*, 461−472.
29. Oe, H., Doi, E., and Hirose, M. (1988) *J. Biochem. 103*, 1066−1072.
30. Ramakrishnan, C., and Ramachandran, G. N. (1965) *Biophys. J. 5*, 909−933.

31. Gerstein, M., Anderson, B. F., Norris, G. E., Baker, E. N., Lesk, A. M., and Chothia, C. (1993) *J. Mol. Biol. 234*, 357−372.
32. Anderson, B. F., Baker, H. M., Norris, G. E., Rumball, S. V., and Baker, E. N. (1990) *Nature 344*, 784−787.
33. Jameson, G. B., Anderson, B. F., Norris, G. E., Thomas, D. H., and Baker, E. N. (1998) *Acta Crystallogr. D54*, 1319−1335.
34. Sharma, A. K., Rajashankar, K. R., Yadav, M. P., and Singh, T. P. (1999) *Acta Crystallogr. D55*, 1152−1157.
35. Morgan, E. H. (1979) *Biochim. Biophys. Acta 580*, 312−326.
36. Bali, P. K., Zak, O., and Aisen, P. (1991) *Biochemistry 30*, 324−328.
37. Steinlein, L. M., Ligman, C. M., Kessler, S., and Ikeda, R. A. (1998) *Biochemistry 37*, 13696−13703.
38. Li, Y., Harris, W. R., Maxwell, A., MacGillivray, R. T. A., and Brown, T. (1998) *Biochemistry 37*, 14157−14166.
39. He, Q.-Y., Mason, A. B., Tam, B. M., MacGillivray, R. T. A., and Woodworth, R. C. (1999) *Biochemistry 38*, 9704−9711.
40. Cheng, Y., Mason, A., and Woodworth, R. C. (1995) *Biochemistry 34*, 14879−14884.
41. Mizutani, K., Yamashita, H., Kurokawa, H., Mikami, B., and Hirose, M. (1999) *J. Biol. Chem. 274*, 10190−10194.
42. Zak, O., Aisen, P., Crawley, J. B., Joannou, C. L., Patel, K. J., Rafiq, M., and Evans, R. W. (1995) *Biochemistry 34*, 14428−14434.
43. Kraulis, P. J. (1991) *J. Appl. Crystallogr. 24*, 946−950.
44. Merritt, E. A., and Bacon, D. J. (1997) *Methods Enzymol. 277*, 505−524.

BI992574Q